# Investigation of magnetic order in Sm$Tr_2Zn_{20}$ ($Tr$ = Fe, Co, Ru) and Sm$Tr_2Cd_{20}$ ($Tr$ = Ni, Pd)

D. Yazici,[1,2] B. D. White,[1,2] P.-C. Ho,[3] N. Kanchanavatee,[1,2] K. Huang,[1,2,4] A. J. Friedman,[1,2] A. S. Wong,[1,2] V. W. Burnett,[1,2] N. R. Dilley,[5] and M. B. Maple[1,2,4,*]

[1]*Department of Physics, University of California, San Diego, La Jolla, California 92093, USA*
[2]*Center for Advanced Nanoscience, University of California, San Diego, La Jolla, California 92093, USA*
[3]*Department of Physics, California State University Fresno, Fresno, California 93740, USA*
[4]*Materials Science and Engineering Program, University of California, San Diego, La Jolla, California 92093, USA*
[5]*Quantum Design, 6325 Lusk Boulevard, San Diego, California 92121, USA*

(Received 8 July 2014; revised manuscript received 16 September 2014; published 3 October 2014)

Single crystals of the "cage compounds" Sm$Tr_2Zn_{20}$ ($Tr$ = Fe, Co, Ru) and Sm$Tr_2Cd_{20}$ ($Tr$ = Ni, Pd) have been investigated by means of electrical resistivity, magnetization, and specific-heat measurements. The compounds $SmFe_2Zn_{20}$, $SmRu_2Zn_{20}$, and $SmNi_2Cd_{20}$ exhibit ferromagnetic order with Curie temperatures of $T_C$ = 47.4, 7.6, and 7.5 K, respectively, whereas $SmPd_2Cd_{20}$ is an antiferromagnet with a Néel temperature of $T_N$ = 3.4 K. No evidence for magnetic order is observed in $SmCo_2Zn_{20}$ down to 110 mK. The Sommerfeld coefficients $\gamma$ are found to be 57 mJ/mol K$^2$ for $SmFe_2Zn_{20}$, 79.5 mJ/mol K$^2$ for $SmCo_2Zn_{20}$, 258 mJ/mol K$^2$ for $SmRu_2Zn_{20}$, 165 mJ/mol K$^2$ for $SmNi_2Cd_{20}$, and 208 mJ/mol K$^2$ for $SmPd_2Cd_{20}$. Enhanced values of $\gamma$ and a quadratic temperature dependence of the electrical resistivity at low temperature for $SmRu_2Zn_{20}$ and $SmPd_2Cd_{20}$ suggest an enhancement of the quasiparticle masses due to hybridization between localized 4$f$ and conduction electron states.

DOI: 10.1103/PhysRevB.90.144406 PACS number(s): 71.27.+a, 72.15.Eb, 75.30.Mb, 75.50.Cc

## I. INTRODUCTION

Intermetallic compounds containing Sm have attracted significant interest for displaying a large variety of unusual physical phenomena. For example, SmS undergoes an isostructural first-order electronic phase transition to a collapsed gold phase that exhibits "valence fluctuation" behavior [1,2], the $La_{1-x}Sm_xSn_3$ system displays Kondo anomalies in superconducting and normal-state properties [3,4], and $SmB_6$ has an intermediate Sm valence and is a hybridization gap semiconductor (Kondo insulator) [5]. Among the Sm-based filled skutterudite compounds, $SmOs_4Sb_{12}$ displays a heavy-fermion state that is robust against applied magnetic field [6–10], $SmFe_4P_{12}$ exhibits ferromagnetic order [11], and $SmRu_4P_{12}$ undergoes a metal-insulator transition associated with multipolar order [12].

The class of intermetallic compounds $RTr_2X_{20}$ ($R$ = rare earth, $Tr$ = transition metal, and $X$ = Al, Zn, Cd), crystallizes in the $CeCr_2Al_{20}$-type ($Fd\bar{3}m$ space group) cubic structure [13–17]. These $RTr_2X_{20}$ compounds have recently attracted much attention because of their unique crystal structure, in which $R$ ions are encapsulated in the Frank-Kasper cages formed by 16 $X$ ions, and have a larger coordination number of tetrahedral groupings of spheres [18], compared to the filled skutterudites and rare-earth hexaborides [19–30]. This crystal structure provides an opportunity to study strongly correlated electronic states, which can be associated with either $f$ or $d$ electrons, and localized rare-earth magnetic moments that have a large spatial separation.

The only Sm-based $RTr_2X_{20}$ compounds to be characterized in single-crystalline form are Sm$Tr_2Al_{20}$ ($Tr$ = Ti, V, Cr), which order antiferromagnetically and show heavy-fermion behavior with strong Sm valence fluctuations [31,32]. In order to better understand the Sm$Tr_2X_{20}$ compounds, we examined the thermodynamic and electrical transport properties of four previously unreported compounds: Sm$Tr_2Zn_{20}$ ($Tr$ = Fe, Ru) and Sm$Tr_2Cd_{20}$ ($Tr$ = Ni, Pd) together with $SmCo_2Zn_{20}$. X-ray diffraction (XRD), electrical resistivity, magnetization, and specific-heat measurements revealed a ferromagnetic ground state for $SmFe_2Zn_{20}$, $SmRu_2Zn_{20}$, and $SmNi_2Cd_{20}$ and an antiferromagnetic ground state for $SmPd_2Cd_{20}$. The formation of heavy quasiparticles in the ordered states of the $SmRu_2Zn_{20}$ and $SmPd_2Cd_{20}$ compounds is also observed. Analysis of the low-temperature electrical resistivity data suggests the presence of spin-wave excitations for $SmFe_2Zn_{20}$, $SmRu_2Zn_{20}$, $SmNi_2Cd_{20}$, and $SmPd_2Cd_{20}$.

## II. EXPERIMENTAL DETAILS

Single crystals of Sm$Tr_2Zn_{20}$ ($Tr$ = Fe, Co, Ru), $YFe_2Zn_{20}$, Sm$Tr_2Cd_{20}$ ($Tr$ = Ni, Pd), $YNi_2Cd_{20}$, and $LaNi_2Cd_{20}$ were prepared by the Zn and Cd self-flux methods, respectively. Details of the sample synthesis are described in Refs. [22,33]. Crystal structure and sample quality were primarily characterized through analysis of powder XRD patterns collected by a Bruker D8 x-ray diffractometer. Four-wire electrical resistivity measurements were performed from 300 to ~1.1 K in a pumped $^4$He Dewar for Sm$Tr_2Zn_{20}$ ($Tr$ = Fe, Co, Ru) and $SmPd_2Cd_{20}$, and down to 110 mK using a $^3$He-$^4$He dilution refrigerator for $SmCo_2Zn_{20}$. Electrical resistivity measurements were performed for $SmNi_2Cd_{20}$ down to 0.36 K using an electrical transport option on the $^3$He insert for a Quantum Design Physical Property Measurement System (PPMS) equipped with a 9-T superconducting magnet. Magnetization measurements were performed between 300 and 2 K in a Quantum Design Magnetic Property Measurement System (MPMS) equipped with a 7-T superconducting magnet. Specific-heat measurements were performed down to 1.8 K in a PPMS Dynacool using a standard thermal relaxation

*Corresponding author: mbmaple@ucsd.edu

 

TABLE I. Summary of structural, magnetic, and electrical transport properties for $SmTr_2Zn_{20}$ ($Tr$ = Fe, Co, Ru) and $SmTr_2Cd_{20}$ ($Tr$ = Ni, Pd) compounds. Included in the table are the cubic lattice parameter $a$; Curie-Weiss temperature $\Theta_{CW}$; effective magnetic moment $\mu_{eff}$; magnetic ordering temperature $T_C$ or $T_N$; saturation magnetic moment $\mu_{sat}$ at 5 T along the [111] crystallographic direction; residual resistivity $\rho_0$ measured at $T \sim 1.2$ K for $SmTr_2Zn_{20}$ ($Tr$ = Fe, Co, Ru) and $SmPd_2Cd_{20}$, and $T \sim 0.5$ K for $SmNi_2Cd_{20}$; coefficient of the $T^2$ term of the electrical resistivity $A$ (with temperature range of fit given in parentheses); residual resistivity ratio RRR $\equiv R$ (300 K)/$R$ (1.2 K) for $SmTr_2Zn_{20}$ ($Tr$ = Fe, Ru) and $SmPd_2Cd_{20}$ and RRR $\equiv R$ (300 K)/$R$ (0.5 K) for $SmNi_2Cd_{20}$ and $SmCo_2Zn_{20}$; and spin-wave energy gap $\Delta_{spw}$.

| Compound | $a$ (Å) | $\Theta_{CW}$ (K) | $\mu_{eff}$ ($\mu_B$) | $T_C$ or $T_N$ (K) | $\mu_{sat}$ ($\mu_B$) | $\rho_0$ ($\mu\Omega$ cm) | $A$ ($\frac{\mu\Omega\,cm}{K^2}$) | RRR | $\Delta_{spw}$ (K) |
|---|---|---|---|---|---|---|---|---|---|
| $SmFe_2Zn_{20}$ | 14.51 | 47.8 | 1.7 | 47.4 | 1.05 | 3.5 | $4.41 \times 10^{-3}$ ($T < 4$ K) | 21 | 4.82 |
| $SmCo_2Zn_{20}$ | 14.08 | − 1.83 | 0.99 | | | 5.8 | – | 12 | |
| $SmRu_2Zn_{20}$ | 14.73 | 8.62 | 0.71 | 7.6 | 0.47 | 11.5 | $2.9 \times 10^{-2}$ ($T < 3$ K) | 7.2 | 3.88 |
| $SmNi_2Cd_{20}$ | 15.53 | 56.2 | 0.71 | 7.5 | 0.52 | 0.11 | – | 21 | 8.79 |
| $SmPd_2Cd_{20}$ | 15.56 | − 6.88 | 0.74 | 3.4 | | 0.06 | $4.8 \times 10^{-1}$ ($T < 3$ K) | 80 | 3.63 |

technique. The orientation of single crystals was determined using a Bruker D8 Discover x-ray diffractometer.

## III. RESULTS AND DISCUSSION

Analysis of powder XRD patterns indicated that the single crystals contained no inclusions of impurity phases. Table I lists the results of Rietveld refinements that were conducted on powder XRD patterns for each sample using GSAS [34] and EXPGUI [35]. The $CeCr_2Al_{20}$-type cubic crystal structure with space group $Fd\bar{3}m$ was observed for all samples. A representative XRD pattern (for the $SmNi_2Cd_{20}$ single crystal) is shown in Fig. 1, plotted with its refined pattern for comparison.

Magnetization divided by applied magnetic field $M/H$ data are displayed as a function of temperature in Fig. 2(a). Measurements were performed in applied magnetic fields of $H = 0.1$ T for $SmFe_2Zn_{20}$, $SmRu_2Zn_{20}$, and $SmPd_2Cd_{20}$, $H = 0.5$ T for $SmCo_2Zn_{20}$, and in $H = 0.05$ T for $SmNi_2Cd_{20}$. The $SmFe_2Zn_{20}$, $SmRu_2Zn_{20}$, $SmNi_2Cd_{20}$, and $SmPd_2Cd_{20}$ compounds exhibit features in $M/H$ that are consistent with a magnetic phase transition. $M/H$ data as a function of temperature reveal the primary difference between the Fe column members ($SmFe_2Zn_{20}$ and $SmRu_2Zn_{20}$) and the Co column member ($SmCo_2Zn_{20}$): for Fe column members, there is an apparent ferromagnetic (FM) order (with notably high and moderately high Curie temperature of $T_C = 47.4$ and 7.6 K for $SmFe_2Zn_{20}$ and $SmRu_2Zn_{20}$, respectively). In contrast, no evidence for magnetic order is observed down to 2 K for $SmCo_2Zn_{20}$. However, the large increase in $M/H$ below 10 K for $SmCo_2Zn_{20}$, which does not obey Curie-Weiss law behavior, could in principle be related to magnetic order below 2 K.

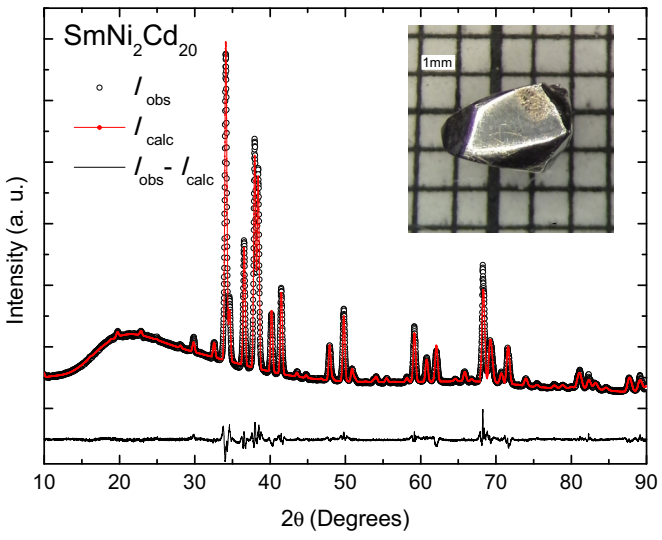


FIG. 1. (Color online) X-ray diffraction pattern for $SmNi_2Cd_{20}$ measured at room temperature. The black open circles indicate the observed intensity $I_{obs}$, the red line represents the calculated intensity $I_{calc}$, and the black line indicates the difference $I_{obs} - I_{calc}$. A broad, featureless hump at low angle comes from the glass slide and petroleum jelly used to mount the powder on the slide. A photograph of a $SmNi_2Cd_{20}$ single crystal is shown in the inset of the figure where the small squares are 1 mm × 1 mm for reference.

Among the $RTr_2Zn_{20}$ compounds, $GdFe_2Zn_{20}$ and $GdCo_2Zn_{20}$ have attracted special attention due to the distinct magnetic properties exhibited by each compound [21,22,36]. $GdFe_2Zn_{20}$ is a FM with a remarkably high Curie temperature of $T_C = 86$ K compared with other $RFe_2Zn_{20}$ compounds. However, as Co is substituted for Fe, ferromagnetic order is rapidly suppressed, culminating in antiferromagnetic (AFM) order at $T_N = 5.7$ K in $GdCo_2Zn_{20}$ [21,36]. Band-structure calculations suggest that the enhanced Curie temperature in $GdFe_2Zn_{20}$ is due to a large $d$-electron contribution to the electronic density of states at the Fermi energy when compared to $GdCo_2Zn_{20}$, and that the transition from FM to AFM order is associated with the filling of electronic states with two additional electrons/f.u [21,36]. $TbFe_2Zn_{20}$ and $TbCo_2Zn_{20}$ also exhibit distinct magnetic behavior according to neutron scattering measurements; $TbFe_2Zn_{20}$ is a ferromagnet with $T_C = 66$ K and $TbCo_2Zn_{20}$ orders antiferromagnetically at $T_N = 2.5$ K [37]. The neutron scattering data are consistent with a picture of the $RFe_2Zn_{20}$ family of compounds in which the high ordering temperatures are associated with the highly polarizable Fe lattice; however, we note that the small magnetic moments on the Fe sites do not order [37]. This distinct magnetic behavior is expected because the rare-earth and transition-metal ions in the $RTr_2Zn_{20}$ compounds are surrounded by Zn cages, preventing direct magnetic exchange interactions between the $4f$ or $3d$ levels. Rather, an indirect Ruderman-Kittel-Kasuya-Yosida (RKKY) [38–41] magnetic exchange interaction, mediated by the conduction electrons, provides the mechanism for magnetic order. Therefore, the

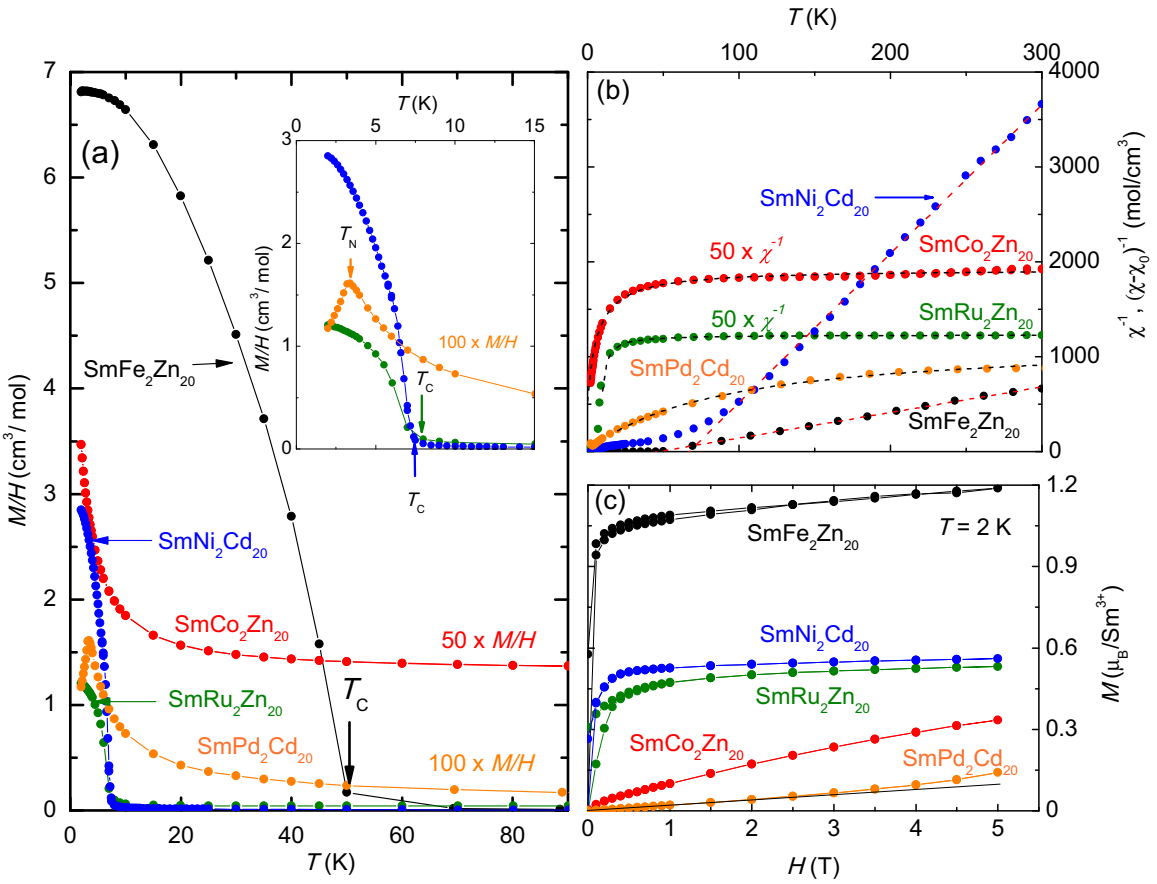


FIG. 2. (Color online) (a) Magnetic susceptibility $M/H$ as a function of temperature $T$ measured in an applied magnetic field of $H = 0.1$ T for $SmFe_2Zn_{20}$, $SmRu_2Zn_{20}$, and $SmPd_2Cd_{20}$, $H = 0.5$ T for $SmCo_2Zn_{20}$, and $H = 0.05$ T for $SmNi_2Cd_{20}$. Inset: low temperature $M/H$ vs. $T$ data for $SmRu_2Zn_{20}$, $SmNi_2Cd_{20}$, and $SmPd_2Cd_{20}$. The magnetic ordering temperatures $T_C$ and $T_N$ are emphasized by arrows. The $M/H$ vs. $T$ data for $SmCo_2Zn_{20}$ and $SmPd_2Cd_{20}$ were scaled by factors of 50 and 100, respectively, for clarity. (b) Inverse magnetic susceptibility data $\chi^{-1} = H/M$ vs. $T$ for Sm$Tr_2$Zn$_{20}$ ($Tr$ = Fe, Co, Ru) and Sm$Tr_2$Cd$_{20}$ ($Tr$ = Ni, Pd). Dashed red lines represent modified Curie-Weiss fits to the data using Eq. (1) and dashed black lines represent the fits to the data using Eq. (2) as described in the text. The $\chi^{-1} = H/M$ vs. $T$ data for $SmCo_2Zn_{20}$ and $SmRu_2Zn_{20}$ were scaled by a factor of 50 for clarity. (c) $M$ vs. $H$ data at $T = 2$ K for the Sm$Tr_2$Zn$_{20}$ ($Tr$ = Fe, Co, Ru) and Sm$Tr_2$Cd$_{20}$ ($Tr$ = Ni, Pd) compounds. The black solid line is a guide to the eye to clarify the separation from the linear behavior of $M$ vs. $H$ data for $SmPd_2Cd_{20}$ at an applied magnetic field of $H = 2.5$ T.

conduction electrons play an important role in controlling the magnetic properties of the $RTr_2Zn_{20}$ compounds.

The remarkable differences in magnetic behavior between $SmCo_2Zn_{20}$ and $SmFe_2Zn_{20}$ could be associated with the fact that there are two extra electrons per formula unit in $SmCo_2Zn_{20}$ than in $SmFe_2Zn_{20}$, in analogy with the $R$ = Gd compounds [21,36]. Interestingly, even though Ni and Pd are in the same column of the periodic table, $SmNi_2Cd_{20}$ and $SmPd_2Cd_{20}$ show different magnetic behavior in their ground states; $SmNi_2Cd_{20}$ has a FM ground state with $T_C = 7.5$ K and $SmPd_2Cd_{20}$ has an AFM ground state with $T_N = 3.4$ K.

Inverse dc magnetic susceptibility $\chi_{dc}^{-1}$ versus $T$ data for $SmFe_2Zn_{20}$ and $SmNi_2Cd_{20}$ were fitted using the Curie-Weiss law

$$\chi - \chi_0 = C_0/(T - \Theta_{CW}), \qquad (1)$$

where $\chi_0$ is a temperature-independent contribution from the filled electron shells and conduction electrons, in the temperature range 60–300 K to determine the Curie-Weiss temperature $\Theta_{CW}$ and effective magnetic moment of the rare-earth site $\mu_{eff}$. The effective moment $\mu_{eff}$ was extracted from the Curie constant $C_0 = N_A\mu_{eff}^2/3k_B$, where $N_A$ is Avogadro's number and $k_B$ is Boltzmann's constant. This analysis was performed by fitting Eq. (1) to the data using nonlinear least-squares regression. The resulting best-fit parameter values for $\mu_{eff}$ and $\Theta_{CW}$ are tabulated in Table I. The theoretical $Sm^{3+}$ free ion magnetic moment is $\mu_{eff} = g_J[J(J+1)]^{1/2}\mu_B = 0.845\mu_B$/f.u., where $g_J = 0.286$ is the Landé $g$ factor and $J = \frac{5}{2}$. The effective moment $\mu_{eff}$ values were determined to be $1.7\mu_B$/f.u. and $0.71\mu_B$/f.u. for $SmFe_2Zn_{20}$ and $SmNi_2Cd_{20}$, respectively, which are larger for $SmFe_2Zn_{20}$ and somewhat smaller for $SmNi_2Cd_{20}$ than the theoretical $Sm^{3+}$ free ion value. It has been reported that $DyFe_2Zn_{20}$ is a ferrimagnet with a magnetic moment associated with both Dy and Fe via Mössbauer experiments [20]. This might be the reason for the larger $\mu_{eff}$ value of $SmFe_2Zn_{20}$: both Sm and Fe may have magnetic moments in this compound. The positive values of $\Theta_{CW} = 47.8$ K for $SmFe_2Zn_{20}$ and 56.2 K for $SmNi_2Cd_{20}$ are consistent with ferromagnetic interactions.

However, the magnitude of $\Theta_{CW}$ for $SmNi_2Cd_{20}$ is a factor of ~7.5 larger than $T_C$. This observation may suggest the presence of magnetic frustration or a competition between FM and another ordered state in this compound.

On the other hand, $\chi_{dc}^{-1}$ versus $T$ data for $SmCo_2Zn_{20}$, $SmRu_2Zn_{20}$, and $SmPd_2Cd_{20}$ show an extremely weak $T$ dependence with distinctly non–Curie-Weiss behavior. This is common in Sm-containing compounds since $Sm^{3+}$ ions have relatively low-energy angular momentum excited states above the Hund's rule $J = \frac{5}{2}$ ground state. A simple Curie-Weiss law was, therefore, unable to adequately describe the data. Although possible reasons for this weak $T$ dependence include valence fluctuations of Sm ions, the origin is not yet well understood. Similar weak $T$ dependence was also observed in $SmTr_2Al_{20}$ compounds with $3d$ transition metals [31,32]. Previous work has shown that $\chi(T)$ for Sm compounds can often be reasonably well described, without considering splitting of the Sm multiplet by the crystalline electrical field (CEF), by the equation [10,42]

$$\chi(T) = \frac{N_A}{k_B}\left[\frac{\mu_{\text{eff}}^2}{3(T-\theta_{CW})} + \frac{\mu_B^2}{\delta}\right], \qquad (2)$$

where $\mu_B$ is the Bohr magneton, $\delta = 7\Delta/20$, and $\Delta$ is the energy (expressed in units of K) between the Hund's rule $J = \frac{5}{2}$ ground state and the $J = \frac{7}{2}$ first excited state. Equation (2) consists of a Curie-Weiss term due to the $J = \frac{5}{2}$ ground-state contribution and a temperature-independent Van Vleck term due to coupling with the first excited $J = \frac{7}{2}$ multiplet. The best overall fit of Eq. (2) to the $\chi_{dc}^{-1}(T)$ data is shown in Fig. 2(b) (dashed black lines). It can be seen that the free-ion Van Vleck term, without adding a Pauli paramagnetic term, provides an excellent fit to the temperature-independent region at high temperatures. The contribution below 100 K displays Curie-Weiss behavior and fits yield $\mu_{\text{eff}}$ values of $0.99\mu_B$/f.u., $0.71\mu_B$/f.u., and $0.74\mu_B$/f.u. with $\Theta_{CW}$ values of $-1.83$, 8.62, and $-6.88$ K for $SmCo_2Zn_{20}$, $SmRu_2Zn_{20}$, and $SmPd_2Cd_{20}$, respectively. The signs of the $\Theta_{CW}$ values are consistent with ferromagnetic interactions in $SmRu_2Zn_{20}$ ($T_C = 7.6$ K) and antiferromagnetic interactions in $SmPd_2Cd_{20}$ ($T_N = 3.4$ K). The signs of $\Theta_{CW}$ for $SmCo_2Zn_{20}$ imply that there are weak antiferromagnetic interactions in that compound, which is consistent with previous reports [19,22]. However, there are deviations in the $\mu_{\text{eff}}$ values from the free-ion effective paramagnetic moment of $0.845\mu_B$/f.u. We obtain a larger value for $SmCo_2Zn_{20}$ and smaller values for $SmRu_2Zn_{20}$ and $SmPd_2Cd_{20}$. The resulting $\Delta$ values are 412, 265, and 1488 K for $SmCo_2Zn_{20}$, $SmRu_2Zn_{20}$, and $SmPd_2Cd_{20}$, respectively. These values for $SmCo_2Zn_{20}$ and $SmRu_2Zn_{20}$ are much lower than the $\Delta \sim 1500$ K value estimated for free $Sm^{3+}$ ions [43]. However, low values of $\Delta$ have previously been inferred from the fits to $\chi_{dc}(T)$ data for other Sm-based compounds such as $SmRh_4B_4$ ($\Delta = 1080$ K) and $SmOs_4Sb_{12}$ ($\Delta = 850$ K) [10,42].

The nature of the magnetic order in these compounds was further studied by measurements of the isothermal magnetization at low temperatures. Magnetization $M$ versus $H$ data, measured at 2 K with $H$ parallel to the [111] direction, are presented in Fig. 2(c). For $SmFe_2Zn_{20}$, $SmRu_2Zn_{20}$, and $SmNi_2Cd_{20}$, $M(H)$ is consistent with a FM state with a rapid rise and saturation of the ordered moment as the magnetic field increases. By extrapolating the high-field slope of the magnetization curves at 2 K back to $H = 0$ T, the saturation moment $\mu_{\text{sat}}$ was determined to be $1.05\mu_B$/f.u. for $SmFe_2Zn_{20}$; this value is higher than the theoretical value of $M_{\text{sat}} = g_J J\mu_B = 0.71\mu_B$/f.u. We also obtain values of 0.47 and $0.52\mu_B$/f.u., for $SmRu_2Zn_{20}$ and $SmNi_2Cd_{20}$, respectively, which are ~70% of the theoretical value of the free $Sm^{3+}$ ion. The ratio of the effective magnetic moment to the saturation magnetic moment for these compounds is $\mu_{\text{eff}}/\mu_{\text{sat}} \sim 1$, indicating that the $f$ electrons associated with the Sm magnetic moments are localized [44]. At 2 K, the remnant magnetization $M_R$ is 0.58, 0.31, and $0.27\mu_B$/f.u. for $SmFe_2Zn_{20}$, $SmRu_2Zn_{20}$, and $SmNi_2Cd_{20}$, respectively. The $M(H)$ isotherms at temperatures higher than their respective $T_C$'s (not shown here) are approximately linear. On the other hand, $M$ versus $H$ data measured at 2 K are hysteretic for $SmFe_2Zn_{20}$, $SmRu_2Zn_{20}$, and $SmNi_2Cd_{20}$; however, negative curvature for $SmCo_2Zn_{20}$, which cannot be described by Brillouin function and approximately linear behavior for $SmPd_2Cd_{20}$ up to $H = 2.5$ T, is consistent with AFM correlations which can be field stabilized to fully saturated states in large enough applied magnetic fields. A magnetic field of $H = 5$ T was unable to saturate the magnetic moments of the $SmCo_2Zn_{20}$ and $SmPd_2Cd_{20}$ compounds. There is a departure from the linear behavior of $M$ versus $H$ data for $SmPd_2Cd_{20}$ at an applied magnetic field of $H = 2.5$ T, which may be related with classical spin reorientation in a cubic symmetry coordination (i.e., an incipient metamagnetic phase transition).

The electrical resistivity $\rho$ versus temperature $T$ data for the $SmTr_2Zn_{20}$ ($Tr$ = Fe, Co, Ru) and $SmNi_2Cd_{20}$ compounds are displayed in Fig. 3. Metallic behavior is observed for all of the compounds. The zero-field residual resistivity ratios RRR $\equiv R$ (300 K)/$R$ (1.2 K) for $SmTr_2Zn_{20}$ ($Tr$ = Fe, Ru) and $SmPd_2Cd_{20}$, RRR $\equiv R$ (300 K)/$R$ (0.05 K) for $SmNi_2Cd_{20}$, and RRR $\equiv R$ (300 K)/$R$ (0.11 K) for $SmCo_2Zn_{20}$ were found to be ~7–80, which indicates that the single crystals studied are of good metallurgical quality (i.e., low impurity scattering). The values for RRR are given in Table I. A shoulder develops in the zero-field $\rho(T)$ curve for $SmFe_2Zn_{20}$, $SmRu_2Zn_{20}$, $SmNi_2Cd_{20}$, and $SmPd_2Cd_{20}$, below which $\rho(T)$ exhibits a sharp drop, indicating a transition to an ordered state. A similar shoulder with a gentle rolloff can also be seen in the zero-field $\rho(T)$ curve for $SmCo_2Zn_{20}$ (indicated by an arrow in the inset of Fig. 3(a)) without an accompanying sharp drop. The transition temperatures $T_C$ and $T_N$ at which these drops occur are defined as the intercept of two lines, one of which is a linear fit to the data above the transition, while the other is a linear fit to the data below the transition. Examples of this definition of the $T_C$ values are shown in Fig. 3(b) and the resulting values of $T_C$ and $T_N$ are indicated by arrows in the inset of Fig. 3(a). The $T_C$ value for $SmNi_2Cd_{20}$ is determined to be 6.6 K in zero magnetic field, which increases to $T_C = 7.5$ K in an applied magnetic field of $H = 5$ T. This behavior is consistent with a ferromagnetic ground state in $SmNi_2Cd_{20}$, in agreement with our magnetic susceptibility results.

In order to analyze the behavior of the electrical resistivity at low temperature, the $\rho(T)$ data were fit with a power law of the form $\rho = \rho_0 + AT^n$. The best-fit parameter values for $\rho_0$ (selected to maximize the linear region of the $\ln(\rho - \rho_0)$

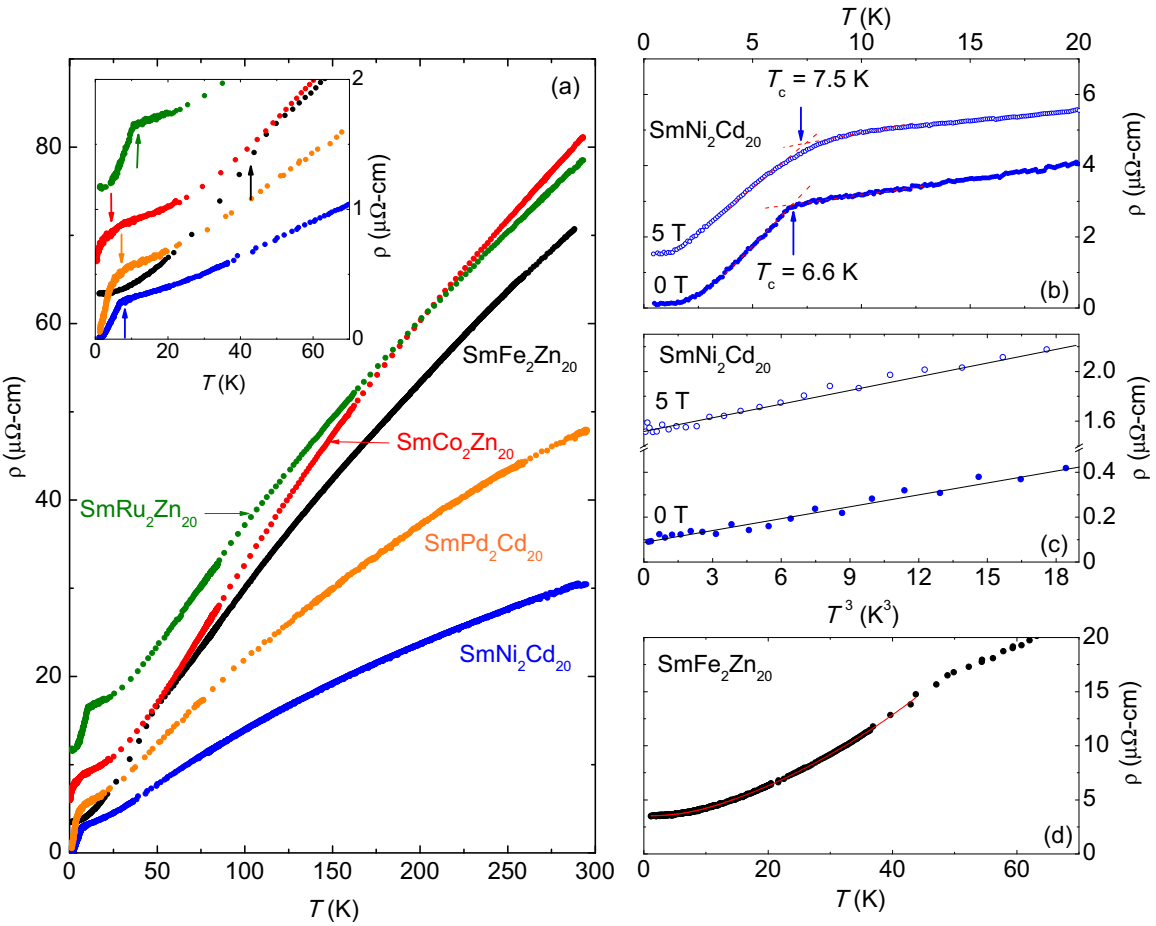


FIG. 3. (Color online) (a) Electrical resistivity $\rho$ vs. temperature $T$ for Sm$Tr_2$Zn$_{20}$ ($Tr$ = Fe, Co, Ru) and Sm$Tr_2$Cd$_{20}$ ($Tr$ = Ni, Pd). Inset: electrical resistivity at low temperatures emphasizing the magnetic ordering temperatures $T_C$ and $T_N$ (indicated by arrows). For $SmCo_2Zn_{20}$, the arrow indicates the low-temperature shoulder in $\rho(T)$. (b) Low-$T$ $\rho$ vs. $T$ data in zero field and an $H = 5$ T applied magnetic field for $SmNi_2Cd_{20}$. The red dashed lines indicate the method we used to determine $T_C$. (c) Low-$T$ $\rho$ vs. $T^3$ data in zero field and an $H = 5$ T applied magnetic field for $SmNi_2Cd_{20}$ with power-law fits (solid black line). (d) Low-$T$ $\rho$ vs. $T$ data in zero magnetic field for $SmFe_2Zn_{20}$ with spin-wave scattering fit (solid red line) using Eq. (3).

versus ln$T$ fit extending from low $T$) and $A$ are listed in Table I. As an example, a best fit for the $SmNi_2Cd_{20}$ data is plotted as a solid line in Fig. 3(c). The residual resistivity $\rho_0$ increases with increasing magnetic field. For both $H = 0$ and 5 T, $n \sim 3$ indicating that $SmNi_2Cd_{20}$ exhibits neither typical Fermi-liquid (FL) ($n \sim 2$) nor typical non-Fermi-liquid (NFL) ($n < 2$) behavior. On the other hand, the exponent values of $n \sim 2$ for $SmFe_2Zn_{20}$, $SmRu_2Zn_{20}$, and $SmPd_2Cd_{20}$ are consistent with a Fermi-liquid state and $n \sim 0.9$ for $SmCo_2Zn_{20}$ is consistent with typical NFL behavior [45,46]. We note that these power-law fits were made to maximum temperatures that are less than the respective spin-wave gap temperatures $\Delta_{spw}$ (see Table I); therefore, scattering with spin waves should be negligible in this analysis and can safely be neglected.

Since ferromagnetic order occurs below $T_C$, electron-spin-wave scattering at higher temperatures was considered with the form [47]

$$\rho(T) = \rho_0 + B\frac{T}{\Delta_{spw}}\left(1 + 2\frac{T}{\Delta_{spw}}\right)\exp\left(-\frac{\Delta_{spw}}{T}\right), \quad (3)$$

where $\Delta_{spw}$ is the spin-wave energy gap, which may result either from magnetic anisotropy or from broken symmetry due to the presence of a CEF. This formula describes the $\rho(T)$ data in a ferromagnetically ordered state. A FL term $AT^2$ was added to Eq. (3) for fits to $SmFe_2Zn_{20}$ and $SmRu_2Zn_{20}$ data. An example of the best fit for $SmFe_2Zn_{20}$ is given in Fig. 3(d). As determined from the fits, the spin-wave energy gap values $\Delta_{spw}$ for $SmFe_2Zn_{20}$, $SmRu_2Zn_{20}$, and $SmNi_2Cd_{20}$ are 4.8, 3.9, and 8.8 K, respectively. However, $SmPd_2Cd_{20}$ orders antiferromagnetically so the following expression was used to fit the spin-wave scattering contribution to electrical resistivity [48,49]:

$$\rho(T) = \rho_0 + AT^2 + C\Delta_{spw}^2\sqrt{\frac{T}{\Delta_{spw}}} \times \left[1 + \frac{2}{3}\left(\frac{T}{\Delta_{spw}}\right) + \frac{2}{15}\left(\frac{T}{\Delta_{spw}}\right)^2\right]e^{-\frac{\Delta_{spw}}{T}}. \quad (4)$$

The differences in the values extracted for $\Delta_{spw}$ via fits to the low-temperature $\rho(T)$ data using Eqs. (3) and (4) are small because the exponential term that contains the gap in its argument is the dominant term in both expressions. However, the values for $\Delta_{spw}$ extracted by using Eq. (4) agree much

better with the values for the energy gap obtained from fits of the low-temperature specific-heat data as discussed below. The spin-wave energy gap $\Delta_{spw}$ for $SmPd_2Cd_{20}$ is determined to be 3.6 K. Because magnetic order is not observed for $SmCo_2Zn_{20}$, it is inappropriate to describe the $\rho(T)$ data with an expression containing spin-wave scattering; therefore, we have limited these fits to the $\rho(T)$ data for $SmFe_2Zn_{20}$, $SmRu_2Zn_{20}$, $SmNi_2Cd_{20}$, and $SmPd_2Cd_{20}$. The extracted values for $\Delta_{spw}$ are reasonably close to one another and are listed in Table I.

Specific heat divided by temperature $C/T$ versus temperature $T$ data are shown in Fig. 4(a). A sharp lambdalike anomaly in $C/T$ is observed at $T_C = 6.76$ K for $SmRu_2Zn_{20}$, $T_C = 6.34$ K for $SmNi_2Cd_{20}$, and $T_N = 3.05$ K for $SmPd_2Cd_{20}$, indicating a second-order phase transition. However, $C/T$ versus $T$ data do not manifest a standard lambdalike anomaly for $SmFe_2Zn_{20}$; rather, they exhibit a broad shoulder around $T_C$, which is taken to be the midpoint of the region with nearly zero slope, and was determined to be $T_C = 44.4$ K. This broad feature is observed more clearly after a background subtraction as shown in Figs. 4(c)–4(e), which may indicate a distribution of $T_C$ values associated with multiple transitions. All of the magnetic ordering temperatures are indicated by arrows in Fig. 4(a). The upturn in $SmCo_2Zn_{20}$ below 10 K may be related to a Schottky anomaly due to splitting of the Hunds's rule ground state of $Sm^{3+}$ by the CEF. Similar results in $C(T)$ data for $SmCo_2Zn_{20}$ were observed by Jia *et al.* [19]. Additionally, we observed another upturn at lower temperatures below 2 K which may also be related to a Schottky anomaly due to splitting of the nuclear states. On the other hand, this upturn might be associated with NFL behavior in $SmCo_2Zn_{20}$, which is supported by the subquadratic temperature dependence of the electrical resistivity below ~2 K. Low-temperature specific-heat measurements are necessary to clarify whether $SmCo_2Zn_{20}$ has a NFL or a FL ground state in which the properties below 10 K are dominated by spin fluctuations. It is of interest to note that a broad shoulder below $T_C$ and $T_N$ is a common feature in compounds such as $TbCo_2Zn_{20}$, $ErFe_2Zn_{20}$, and $PrTi_2Al_{20}$ [19,50]. According to calculations by Fishman and Liu [51], these features arise naturally in a Heisenberg ferromagnet with large spin quantum number; however, it is also possible for quantum fluctuations in the transverse degrees of freedom to produce similar features [51].

The electronic and phonon contributions to specific heat, characterized by $\gamma$ and $\beta$, respectively, were determined by linear fits to the data plotted as $C/T$ versus $T^2$ using the expression $C/T = \gamma + \beta T^2$. The fits were performed in the 100–250 $K^2$ temperature range to avoid contributions from magnetic order below 10 K or Schottky anomalies for $SmCo_2Zn_{20}$, $SmRu_2Zn_{20}$, $SmNi_2Cd_{20}$, and $SmPd_2Cd_{20}$. The $\gamma$ values of $SmCo_2Zn_{20}$, $SmRu_2Zn_{20}$, $SmNi_2Cd_{20}$, and

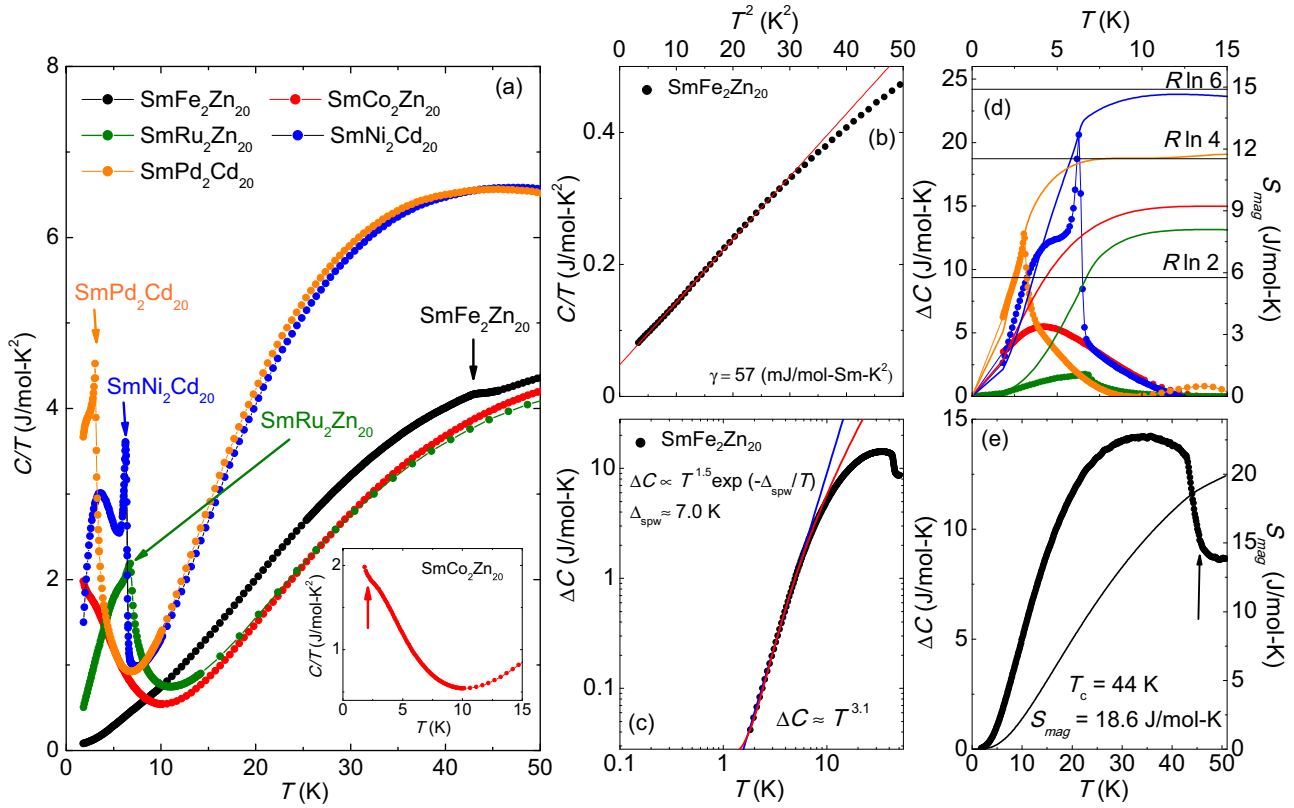


FIG. 4. (Color online) (a) Specific heat divided by temperature, $C/T$, for $SmTr_2Zn_{20}$ ($Tr$ = Fe, Co, Ru) and $SmNi_2Cd_{20}$ in zero magnetic field. Arrows refer to magnetic phase transition temperatures. Inset: $C/T$ for $SmCo_2Zn_{20}$ emphasizing the upturn at low temperatures below 2 K (indicated by the arrow). (b) $C/T$ vs. $T^2$ for $SmFe_2Zn_{20}$. The solid line represents a fit to the data using the equation $C/T = \gamma + \beta T^2$. (c) Logarithmic plot of power-law fit (blue solid line) and anisotropic spin-wave fit (red solid line) to the magnetic contribution to the specific heat, $\Delta C(T)$, for $SmFe_2Zn_{20}$ after electronic and lattice contributions have been subtracted. (d) Magnetic entropy, $S_{mag}$, vs. $T$ for $SmTr_2Zn_{20}$ ($Tr$ = Co, Ru) and $SmNi_2Cd_{20}$. (e) Magnetic contribution to specific heat, $\Delta C$, (corresponds to left axis) and the magnetic entropy, $S_{mag}$, (right axis) vs. $T$ for $SmFe_2Zn_{20}$.

TABLE II. Summary of characteristic quantities and ratios for $RTr_2Zn_{20}$ ($R$ = Y, La, Sm, $Tr$ = Fe, Co, Ru) and $RTr_2Cd_{20}$ ($R$ = Y, La, Sm, $Tr$ = Ni, Pd). Included in the table are the Sommerfeld coefficient of the specific heat $\gamma$; Sommerfeld-Wilson ratio SWR; and Kadowaki-Woods ratio KWR.

| Compound | $\gamma$ ($\frac{\text{mJ}}{\text{mol K}^2}$) | SWR | KWR ($\frac{\mu\Omega\,\text{cm mol}^2\,\text{K}^2}{\text{mJ}^2}$) |
|---|---|---|---|
| $YFe_2Zn_{20}$ | 53 | | |
| $YNi_2Cd_{20}$ | 22.9 | | |
| $LaNi_2Cd_{20}$ | 25.9 | | |
| $SmFe_2Zn_{20}$ | 57 | | |
| $SmCo_2Zn_{20}$ | 79.5 | | |
| $SmRu_2Zn_{20}$ | 258 | 2.0 | $4.4 \times 10^{-7}$ |
| $SmNi_2Cd_{20}$ | 165 | | |
| $SmPd_2Cd_{20}$ | 208 | 0.7 | $1.1 \times 10^{-5}$ |

$SmPd_2Cd_{20}$ are listed in Table II together with $\gamma$ values for nonmagnetic $YFe_2Zn_{20}$, $YNi_2Cd_{20}$, and $LaNi_2Cd_{20}$ reference compounds [30,33]. These values of $\gamma$ are upper limits, and their precise values are subject to some uncertainty because of experimental constraints imposed by the low-temperature upturn of $C/T$ for $SmCo_2Zn_{20}$ and the sharp lambdalike anomalies for $SmRu_2Zn_{20}$, $SmNi_2Cd_{20}$, and $SmPd_2Cd_{20}$. An example of the linear fit for $SmFe_2Zn_{20}$ is shown in Fig. 4(b) as a solid line; the fit was performed in the 4–25 $K^2$ temperature range. Sommerfeld coefficient values of $\gamma \sim 57$ mJ/mol $K^2$ for $SmFe_2Zn_{20}$, $\sim$79.5 mJ/mol $K^2$ for $SmCo_2Zn_{20}$, $\sim$258 mJ/mol $K^2$ for $SmRu_2Zn_{20}$, $\sim$165 mJ/mol $K^2$ for $SmNi_2Cd_{20}$, and $\sim$208 mJ/mol $K^2$ for $SmPd_2Cd_{20}$ were obtained.

In general, $\gamma$ is proportional to the total density of states at the Fermi energy $D(E_f)$. The observed differences between $\gamma$ values probably simply reflect differences in the electronic structure of these compounds. On average, the compounds with $X$ = Cd appear to have larger values of $\gamma$ than when $X$ = Zn, and the $\gamma$ values also seem to increase when we go from 3$d$ to 4$d$ transition-metal elements. For clarity, it would be helpful to perform band-structure calculations. Since there are 23 atoms per formula unit in these 1-2-20 compounds, the electronic states coming from the transition metal and Zn or Cd ions could produce a fairly large contribution to $D(E_f)$ without considering any Sm contributions. We have, therefore, compared the $\gamma$ values we measure for the Sm-based compounds with values obtained from suitable nonmagnetic reference compounds where $R$ = Y or La. The difference between these values is a measure of the contribution of Sm and its interactions with itinerant electron states (i.e., any quasiparticle resonances) to $D(E_f)$. The electronic specific-heat coefficient $\gamma$ (see Table II) for $SmFe_2Zn_{20}$ and $SmCo_2Zn_{20}$ is not very different from the $\gamma$ value of nonmagnetic $YFe_2Zn_{20}$. However, there is an enhancement of the $\gamma$ value for $SmRu_2Zn_{20}$, $SmNi_2Cd_{20}$, and $SmPd_2Cd_{20}$ relative to the $\gamma$ value of $YRu_2Zn_{20}$ ($\gamma \sim$ 34 mJ/mol $K^2$) [22], $YFe_2Zn_{20}$, $YNi_2Cd_{20}$, and $LaNi_2Cd_{20}$, indicating an enhancement of $D(E_f)$ associated with Sm ions. The Debye temperature $\Theta_D$ was calculated using the relation $\Theta_D = [23 * 1944 * 1000(1/\beta)]^{1/3}$ K. For all of the compounds studied, $\Theta_D$ values are roughly the same near $\sim$214 K.

Figure 4(c) displays the magnetic contribution to specific heat $\Delta C(T)$ of $SmFe_2Zn_{20}$ as a representative example. $\Delta C(T)$ is obtained after the specific heat of nonmagnetic $YFe_2Zn_{20}$, $LaNi_2Cd_{20}$ (used to estimate the lattice contribution to specific heat for $SmFe_2Zn_{20}$ and $SmNi_2Cd_{20}$, respectively) is subtracted from the specific heat of $SmFe_2Zn_{20}$ and $SmNi_2Cd_{20}$, respectively, and $\gamma T + \beta T^3$ (estimated electronic and lattice contribution terms) is subtracted from the specific heats of $SmRu_2Zn_{20}$ and $SmPd_2Cd_{20}$. The low-temperature data for $SmFe_2Zn_{20}$, $SmRu_2Zn_{20}$, and $SmNi_2Cd_{20}$ were fit with a spin-wave formula $\Delta C(T) \propto T^n$, which is appropriate for magnetically isotropic metals. Fits were made using $\Delta C(T) \propto T^{3/2} \exp(-\Delta_{spw}/T)$ for magnetically anisotropic metals, and $\Delta C(T) \propto T^3 \exp(-\Delta_{spw}/T)$ for $SmPd_2Cd_{20}$ [52]. From the first formula, we obtained exponent values of $n \sim$ 3.1, 3.11, 2.8, and 2.9 for $SmFe_2Zn_{20}$, $SmRu_2Zn_{20}$, $SmNi_2Cd_{20}$, and $SmPd_2Cd_{20}$, respectively. These values for $SmFe_2Zn_{20}$, $SmRu_2Zn_{20}$, and $SmNi_2Cd_{20}$ are in disagreement with predictions from theoretical calculations involving ferromagnetic spin waves which yield a $T^{3/2}$ dependence, but they are consistent with a calculation for the specific heat that involves antiferromagnetic spin waves which gives $C \propto T^3$ [53]. The spin-wave energy gap $\Delta_{spw}$ values were determined from the second formula to be 7.0, 4.9, 10.8, and 5.7 K for $SmFe_2Zn_{20}$, $SmRu_2Zn_{20}$, $SmNi_2Cd_{20}$, and $SmPd_2Cd_{20}$, respectively. These values are consistent (i.e., of the same order of magnitude) with the values of 4.8, 3.9, 8.8, and 3.6 K, which were determined from the zero-field electrical resistivity data.

The magnetic contribution to specific heat $\Delta C(T)$ of $SmCo_2Zn_{20}$, $SmRu_2Zn_{20}$, $SmNi_2Cd_{20}$, and $SmPd_2Cd_{20}$ is displayed in Fig. 4(d) (left axis). The magnetic contribution to the entropy $S_{\text{mag}} = \int(\Delta C/T)dT$ (extrapolating a power-law $T$ dependence of $\Delta C/T$ to 0 K to estimate the magnetic entropy below 1.8 K) is displayed in Fig. 4(d) (corresponding to the right axis). The entropy $S_{\text{mag}}$ attains a value of $S_{\text{mag}} \sim$ 5.95 J $\text{mol}^{-1}$ $\text{K}^{-1}$ for $SmRu_2Zn_{20}$, $S_{\text{mag}} \sim$ 12.8 J $\text{mol}^{-1}$ $\text{K}^{-1}$ for $SmNi_2Cd_{20}$, and $S_{\text{mag}} \sim$ 7.81 J $\text{mol}^{-1}$ $\text{K}^{-1}$ for $SmPd_2Cd_{20}$ at their respective magnetic ordering temperatures. Then, $S_{\text{mag}}$ reaches a value of 9.14 J $\text{mol}^{-1}$ $\text{K}^{-1}$ and 8.1 J $\text{mol}^{-1}$ $\text{K}^{-1}$ by 15 K and saturates for $SmCo_2Zn_{20}$ and $SmRu_2Zn_{20}$, respectively. These values are lower than expected for $Sm^{3+}$ with $J = \frac{5}{2}$ ($S_{\text{mag}} = R\ln(2J+1) = 14.9$ J $\text{mol}^{-1}$ $\text{K}^{-1}$) with full degeneracy, but $S_{\text{mag}}$ reaches $\sim R$ ln2 at $T_C = 6.76$ K, which suggests that the ground state of Sm for $SmRu_2Zn_{20}$ could be a $\Gamma_7$ doublet; however, low-temperature specific-heat measurements are necessary to identify the ground state for $SmCo_2Zn_{20}$ because of the low-temperature upturn below 10 K. On the other hand, $S_{\text{mag}} \sim$ 14.7 J $\text{mol}^{-1}$ $\text{K}^{-1}$ at 15 K for $SmNi_2Cd_{20}$ nearly reaches $R$ ln6, indicating that the expected magnetic entropy is completely recovered by this temperature. A value of $S_{\text{mag}} \sim$ 11.7 J $\text{mol}^{-1}$ $\text{K}^{-1}$ at 15 K for $SmPd_2Cd_{20}$ and a value of 7.81 J $\text{mol}^{-1}$ $\text{K}^{-1}$ at $T_N = 3.4$ K suggests that the ground state of Sm in this compound is probably a $\Gamma_8$ quartet [54]. Thus, our check demonstrates that the estimated $\Delta C/T$ curves for the Sm$Tr_2$Zn$_{20}$ ($Tr$ = Fe, Co, Ru) and Sm$Tr_2$Cd$_{20}$ ($Tr$ = Ni, Pd) compounds are reasonable. The sizable release of magnetic entropy indicates that the valence of Sm ions is close to 3+. On the other hand, $S_{\text{mag}}$ versus $T$ for $SmFe_2Zn_{20}$, displayed in Fig. 4(e), attains a value

18.7 J mol$^{-1}$ K$^{-1}$ above the ferromagnetic transition. This is a larger value than expected for $Sm^{3+}$, which may be due to a contribution from Fe ions to the magnetic entropy. Such a scenario is in concert with the larger $\mu_{\rm eff}$ value for $SmFe_2Zn_{20}$ than expected for the $Sm^{3+}$ ion alone.

## IV. DISCUSSION

The magnetic, electrical transport, and thermodynamic properties of $SmFe_2Zn_{20}$, $SmRu_2Zn_{20}$, and $SmNi_2Cd_{20}$ reveal ferromagnetic order below $T_C = 47.4$, 7.6, and 7.5 K, respectively. Antiferromagnetic order is observed below $T_N = 3.4$ K for $SmPd_2Cd_{20}$, but no evidence for magnetic order is observed down to 110 mK for $SmCo_2Zn_{20}$. Magnetic order with low transition temperatures or no ordering at all might be expected in the $RTr_2Zn_{20}$ series of compounds due to their very low rare-earth ion concentrations and large spatial separations between neighboring $R$ ions. However, $SmFe_2Zn_{20}$ exhibits a relatively high Curie temperature of $T_C = 47.4$ K. In the $RTr_2Zn_{20}$ compounds, the rare-earth and transition-metal ions are surrounded by Zn cages preventing direct magnetic exchange interactions between the $4f$ or $3d$ electrons; however, $3d$ electrons from Fe sites in $RFe_2Zn_{20}$ act as important mediators via the RKKY interaction and the indirect magnetic exchange interaction between Fe $3d$ electrons enhances the magnetic interactions between $R^{3+}$ localized magnetic moments, resulting in the remarkably high $T_C$ for $RFe_2Zn_{20}$ compounds. It has also been suggested that the magnetic exchange interaction between the two $R$ ions is weaker than that between $R$ and Fe ions [55]. In this scenario, the $T_C$ of $RFe_2Zn_{20}$ compounds is enhanced by the magnetic exchange interaction between $R$ and Fe ions [55]. The $T_C$ values in the $RFe_2Zn_{20}$ series of compounds with $R$ = Gd-Lu are reported to scale with the de Gennes factor [56], and the relatively high $T_C$ value we observe for $SmFe_2Zn_{20}$ fits in with this scaling behavior of the heavier rare-earth ion members. We note that $RTr_2Zn_{20}$ compounds with $Tr$ = Ru, Os, which are both in the same column as Fe, are characterized by significantly lower $T_C$ values compared to those for $Tr$ = Fe [19]. In the neighboring column, the $RTr_2Zn_{20}$ compounds with $Tr$ = Co, Rh, Ir are known to order antiferromagnetically [19]. Therefore, it appears that the number of conduction electrons from the transition-metal $d$-electron shell plays an important role in determining the magnetic properties of the $RTr_2Zn_{20}$ compounds. However, this conclusion does not appear to apply for all the $RTr_2Cd_{20}$ compounds because, even though Ni and Pd both reside in the same column of the periodic table, $SmNi_2Cd_{20}$ orders ferromagnetically with $T_C = 7.5$ K while $SmPd_2Cd_{20}$ has an antiferromagnetic ground state with $T_N = 3.4$ K. Calculations of the electronic band structure would be helpful to understand why the magnetic structures for $SmNi_2Cd_{20}$ and $SmPd_2Cd_{20}$ are different.

The electronic specific-heat coefficient $\gamma$ (see values of $\gamma$ listed in Table II) for $SmFe_2Zn_{20}$ and $SmCo_2Zn_{20}$ is not significantly larger than the $\gamma$ value for nonmagnetic $YFe_2Zn_{20}$ and $YCo_2Zn_{20}$ ($\gamma \sim 18.3$ mJ/mol K$^2$) [22]. This observation suggests that the electronic structure and the well-localized nature of $4f$ electrons are quite similar in these compounds. However, an enhancement of the $\gamma$ value for $SmRu_2Zn_{20}$, $SmNi_2Cd_{20}$, and $SmPd_2Cd_{20}$, relative to the $\gamma$ values for $YRu_2Zn_{20}$ ($\gamma \sim 34$ mJ/mol K$^2$) [22], $YNi_2Cd_{20}$, and $LaNi_2Cd_{20}$, suggests that heavy quasiparticles form at low temperature or that there is a peak in the electronic density of states $D(E)$ near $E_F$ contributed by Sm states. Since we were unable to prepare nonmagnetic reference compounds for $SmPd_2Cd_{20}$, we assumed that the density of states of $YNi_2Cd_{20}$, $LaNi_2Cd_{20}$, $YPd_2Cd_{20}$, and $LaPd_2Cd_{20}$ are similar. Values of $\gamma$ that are significantly enhanced relative to those of nonmagnetic analogues imply that the $f$ electrons are strongly admixed with conduction-electron states and have developed delocalized character. However, the value $n \sim 3$ of the exponent from the power-law fit of the electrical resistivity data for $SmNi_2Cd_{20}$ and the localized character of $f$ electrons (determined from $\mu_{\rm eff}/\mu_{\rm sat} \sim 1$) [44] in $SmRu_2Zn_{20}$ and $SmNi_2Cd_{20}$ are inconsistent with typical heavy-fermion (HF) physics. Localized $f$ electrons in $SmRu_2Zn_{20}$ and $SmNi_2Cd_{20}$ participate in their respective FM ground states via the RKKY interaction [39–41], which competes with the heavy-fermion state in a generic Doniach model context. This contradictory behavior of $SmRu_2Zn_{20}$ and $SmNi_2Cd_{20}$ suggests that these compounds may be near a ferromagnetic quantum critical point (QCP). Due to the possible proximity to a ferromagnetic QCP, $SmRu_2Zn_{20}$ and $SmNi_2Cd_{20}$ compounds represent potential new model systems for studying the break down of Fermi-liquid behavior near a ferromagnetic QCP. Even though there are extensive studies on HF systems that focus on antiferromagnetic (AFM) QCP's, there are a limited but increasing number of HF ferromagnets (FMs). In particular, Sm-based HF FMs are rare and include $SmFe_4P_{12}$ ($\gamma \sim 350$ mJ/mol K$^2$) [11], $SmOs_4Sb_{12}$ ($\gamma \sim 880$ mJ/mol K$^2$) [9], and SmPtSi ($\gamma \sim 250$ mJ/mol K$^2$) [57]. We also note that a few other Sm-based compounds with the $CeCr_2Al_{20}$-type structure are considered to be heavy fermions with $\gamma \sim 100$ mJ/mol K$^2$ for $SmTi_2Al_{20}$, $\gamma \sim 720$ mJ/mol K$^2$ for $SmV_2Al_{20}$, and $\gamma \sim 1000$ mJ/mol K$^2$ for $SmCr_2Al_{20}$, which all have AFM ground states [31,32]. The investigation of other FM compounds near a QCP is therefore highly desirable for a more complete understanding of quantum criticality. An enhanced electronic specific-heat coefficient for $SmPd_2Cd_{20}$, which has as an exponent value of $n \sim 2$, an AFM ground state, and a possible metamagnetic transition at $T = 2$ K and $H \sim 2.5$ T supports an interpretation that this compound is near a QCP with a FL ground state. We want to emphasize that there is no evidence for a coherence temperature in the electrical resistivity data, as would be expected for typical HF compounds. On the other hand, this lack of distinct features in the electrical resistivity $\rho(T)$ has been observed in other Sm-based HF compounds such as $SmFe_4P_{12}$ and $SmOs_4Sb_{12}$ [9,11], and may indicate that the HF composite quasiparticles in these compounds develop through a route different from the standard Kondo-lattice mechanism.

In order to elucidate the character of the HF behavior, we calculated the Kadowaki-Woods ratio KWR $= A/\gamma^2$, where $\gamma$ is the coefficient of the electronic specific heat and $A$ is the coefficient of the $T^2$ contribution to the electrical resistivity [58]. Calculations were performed for the compounds that have a quadratic $T$ dependence at low temperature in electrical resistivity data. Calculated KWR values are given in Table II. In the original treatment [58], KWR $\approx 10^{-5}\ \frac{\mu\Omega\,\mathrm{cm\ mol^2K^2}}{\mathrm{mJ^2}}$, which is almost the same value we

calculate for $SmPd_2Cd_{20}$. More recently, it has been found that a number of HF compounds based on lanthanide or actinide ions other than Ce (e.g., Sm, Eu, Yb, U) exhibit KWR values closer to $A/\gamma^2 = 1.0 \times 10^{-6}$ $\frac{\mu\Omega\,\mathrm{cm\ mol^2K^2}}{\mathrm{mJ^2}}$, which can be explained by taking into account the degeneracy $N$ of the lanthanide or actinide ions [59]. For $SmRu_2Zn_{20}$, KWR is close to $0.36 \times 10^{-6}$ $\frac{\mu\Omega\,\mathrm{cm\ mol^2K^2}}{\mathrm{mJ^2}}$ when we assume $N = 8$, supporting the formation of a magnetic FL ground state. Moreover, we consider the Sommerfeld-Wilson ratio SWR $= [\pi^2 k_B^2/(\mu_{\mathrm{eff}})^2]\chi_0/\gamma$, where $k_B$ is the Boltzmann constant, $\mu_{\mathrm{eff}}$ is the effective magnetic moment, and $\chi_0$ is the enhanced Pauli susceptibility [60]. SWR values are tabulated in Table II. A SWR ratio value of 0.7 is calculated for $SmPd_2Cd_{20}$; this value is very close to 1, which is expected for a free-electron gas [61]. We calculate a value of 2 for $SmRu_2Zn_{20}$, which is consistent with a Kondo system and has been observed in many HF systems. The $f$-electron spin fluctuations presumably enhance $\chi_0$ relative to $\gamma$, which leads to a larger value for the SWR [61,62].

Low-temperature electrical resistivity data suggest the presence of spin-wave excitations below $T_C$ for $SmFe_2Zn_{20}$, $SmRu_2Zn_{20}$, and $SmNi_2Cd_{20}$, and below $T_N$ for $SmPd_2Cd_{20}$. The uncertainty in the ground state of the Sm multiplet energy-level scheme and the microscopic properties of spin-wave excitations may be resolved by performing neutron scattering experiments. However, for such an experiment, it should be noted that both Sm and Cd are strong neutron absorbers; therefore, samples would need to be synthesized using one of the less-absorbing Sm isotopes such as $^{152}$Sm or $^{154}$Sm and a Cd isotope such as $^{114}$Cd [63].

## V. SUMMARY

Measurements of electrical resistivity, magnetization, and specific heat have been performed for single crystals of the caged compounds $SmTr_2Zn_{20}$ ($Tr$ = Fe, Co, Ru) and $SmTr_2Cd_{20}$ ($Tr$ = Ni, Pd). $SmFe_2Zn_{20}$, $SmRu_2Zn_{20}$, and $SmNi_2Cd_{20}$ exhibit ferromagnetic order with Curie temperatures of $T_C = 47.4$, 7.6, and 7.5 K, respectively, while $SmPd_2Cd_{20}$ is an antiferromagnet with $T_N = 3.4$ K. No evidence for magnetic order is observed in $SmCo_2Zn_{20}$ down to 110 mK. Sommerfeld coefficients $\gamma$ of 57 $\mathrm{mJ/mol\,K^2}$ for $SmFe_2Zn_{20}$, 79.5 $\mathrm{mJ/mol\,K^2}$ for $SmCo_2Zn_{20}$, 258 $\mathrm{mJ/mol\,K^2}$ for $SmRu_2Zn_{20}$, 165 $\mathrm{mJ/mol\,K^2}$ for $SmNi_2Cd_{20}$, and $\sim$208 $\mathrm{mJ/mol\,K^2}$ for $SmPd_2Cd_{20}$ are obtained. Enhanced Sommerfeld coefficients relative to nonmagnetic reference compounds and the exponent $n \sim 2$ from the power-law fits of electrical resistivity data for $SmRu_2Zn_{20}$ and $SmPd_2Cd_{20}$ suggest an enhancement of the quasiparticle masses related due to hybridization between localized $4f$ and conduction electron states. Therefore, we suggest that $SmRu_2Zn_{20}$ is a new addition to the rare class of Sm-based HF ferromagnet with a KWR value of $4.4 \times 10^{-7}$ $\frac{\mu\Omega\,\mathrm{cm\ mol^2K^2}}{\mathrm{mJ^2}}$ and a SWR value of 2, which have been observed in many HF Kondo lattice systems.

## ACKNOWLEDGMENTS

Research at UCSD was supported by the U. S. Department of Energy, Office of Basic Energy Sciences, Division of Material Sciences and Engineering under Grant No. DE-FG02-04-ER46105 (sample synthesis and physical properties measurements above 1 K), and the National Science Foundation under Award Grant No. DMR 1206553 (physical properties measurements below 1 K). Research at California State University, Fresno is supported by the National Science Foundation under Grant No. DMR 1104544. Helpful discussions with Professor T. Yanasigawa are gratefully acknowledged.

[1] A. Jayaraman, V. Narayanamurti, E. Bucher, and R. G. Maines, Phys. Rev. Lett. **25**, 1430 (1970).
[2] M. B. Maple and D. Wohlleben, Phys. Rev. Lett. **27**, 511 (1971); *Magnetism and Magnetic Materials*, AIP Conference Proceedings No. 18, edited by C. D. Graham Jr. and J. J. Rhyne (AIP, New York, 1974), p. 447.
[3] S. Bakanowski, J. Crow, and T. Mihalisin, Solid State Commun. **22**, 241 (1977).
[4] L. De Long, R. McCallum, W. Fertig, M. Maple, and J. Huber, Solid State Commun. **22**, 245 (1977).
[5] A. Menth, E. Buehler, and T. H. Geballe, Phys. Rev. Lett. **22**, 295 (1969).
[6] H. Kotegawa, H. Hidaka, Y. Shimaoka, T. Miki, T. C. Kobayashi, D. Kikuchi, H. Sugawara, and H. Sato, J. Phys. Soc. Jpn. **74**, 2173 (2005).
[7] S. Sanada, Y. Aoki, H. Aoki, A. Tsuchiya, D. Kikuchi, H. Sugawara, and H. Sato, J. Phys. Soc. Jpn. **74**, 246 (2005).
[8] A. Yamasaki, S. Imada, H. Higashimichi, H. Fujiwara, T. Saita, T. Miyamachi, A. Sekiyama, H. Sugawara, D. Kikuchi, H. Sato *et al.*, Phys. Rev. Lett. **98**, 156402 (2007).
[9] M. Mizumaki, S. Tsutsui, H. Tanida, T. Uruga, D. Kikuchi, H. Sugawara, and H. Sato, J. Phys. Soc. Jpn. **76**, 053706 (2007).
[10] W. M. Yuhasz, N. A. Frederick, P.-C. Ho, N. P. Butch, B. J. Taylor, T. A. Sayles, M. B. Maple, J. B. Betts, A. H. Lacerda, P. Rogl *et al.*, Phys. Rev. B **71**, 104402 (2005).
[11] N. Takeda and M. Ishikawa, J. Phys.: Condens. Matter **15**, L229 (2003).
[12] M. Yoshizawa, Y. Nakanishi, M. Oikawa, C. Sekine, I. Shirotani, S. R. Saha, H. Sugawara, and H. Sato, J. Phys. Soc. Jpn. **74**, 2141 (2005).
[13] S. Niemann and W. Jeitschko, J. Solid State Chem. **114**, 337 (1995).
[14] T. Nasch, W. Jeitschko, and U. C. Rodewald, Z. Naturforsch. B **52**, 1023 (1997).
[15] V. M. Thiede, W. Jeitschko, S. Niemann, and T. Ebel, J. Alloys Compd. **267**, 23 (1998).
[16] P. Kripyakevich and O. Zarechnyuk, Dopov. Akad. Nauk Ukr. RSR **Ser. A**, 364 (1968).
[17] O. Moze, L. Tung, J. Franse, and K. Buschow, J. Alloys Compd. **268**, 39 (1998).
[18] F. C. Frank and J. S. Kasper, Acta Crystallogr. **11**, 184 (1958).

[19] S. Jia, N. Ni, S. L. Bud'ko, and P. C. Canfield, Phys. Rev. B **80**, 104403 (2009).

[20] Y. Isikawa, T. Mizushima, K. Kumagai, and T. Kuwai, J. Phys. Soc. Jpn. **82**, 083711 (2013).

[21] S. Jia, S. L. Bud'ko, G. D. Samolyuk, and P. C. Canfield, Nat. Phys. **3**, 334 (2007).

[22] S. Jia, N. Ni, S. L. Bud'ko, and P. C. Canfield, Phys. Rev. B **76**, 184410 (2007).

[23] T. Onimaru, K. T. Matsumoto, Y. F. Inoue, K. Umeo, Y. Saiga, Y. Matsushita, R. Tamura, K. Nashimoto, I. Ishii, T. Suzuki *et al.*, J. Phys. Soc. Jpn. **79**, 033704 (2010).

[24] A. Sakai and S. Nakatsuji, J. Phys. Soc. Jpn. **80**, 063701 (2011).

[25] A. Sakai, K. Kuga, and S. Nakatsuji, J. Phys. Soc. Jpn. **81**, 083702 (2012).

[26] T. J. Sato, S. Ibuka, Y. Nambu, T. Yamazaki, T. Hong, A. Sakai, and S. Nakatsuji, Phys. Rev. B **86**, 184419 (2012).

[27] Y. Saiga, K. Matsubayashi, T. Fujiwara, M. Kosaka, S. Katano, M. Hedo, T. Matsumoto, and Y. Uwatoko, J. Phys. Soc. Jpn. **77**, 053710 (2008).

[28] K. Matsubayashi, T. Tanaka, A. Sakai, S. Nakatsuji, Y. Kubo, and Y. Uwatoko, Phys. Rev. Lett. **109**, 187004 (2012).

[29] P. C. Canfield, S. Jia, E. D. Mun, S. L. Bud'ko, G. D. Samolyuk, and M. S. Torikachvili, Physica B (Amsterdam) **403**, 844 (2008).

[30] M. S. Torikachvili, S. Jia, E. D. Mun, S. T. Hannahs, R. C. Black, W. K. Neils, D. Martien, S. L. Bud'ko, and P. C. Canfield, Proc. Natl. Acad. Sci. USA **104**, 9960 (2007).

[31] A. Sakai and S. Nakatsuji, Phys. Rev. B **84**, 201106 (2011).

[32] R. Higashinaka, T. Maruyama, A. Nakama, R. Miyazaki, Y. Aoki, and H. Sato, J. Phys. Soc. Jpn. **80**, 093703 (2011).

[33] V. W. Burnett, D. Yazici, B. D. White, N. R. Dilley, A. J. Friedman, B. Brandom, and M. B. Maple, J. Solid State Chem. **215**, 114 (2014).

[34] A. C. Larson and R. B. Von Dreele, General Structure Analysis System (GSAS).

[35] B. H. Toby, J. Appl. Crystallogr. **34**, 210 (2001).

[36] S. Jia, N. Ni, G. D. Samolyuk, A. Safa-Sefat, K. Dennis, H. Ko, G. J. Miller, S. L. Bud'ko, and P. C. Canfield, Phys. Rev. B **77**, 104408 (2008).

[37] W. Tian, A. D. Christianson, J. L. Zarestky, S. Jia, S. L. Bud'ko, P. C. Canfield, P. M. B. Piccoli, and A. J. Schultz, Phys. Rev. B **81**, 144409 (2010).

[38] J. J. M. Franse and R. J. Radwanski, in *Handbook of Magnetic Materials*, Vol. 7, edited by K. H. J. Buschow (Elsevier, Amsterdam, 1993).

[39] M. A. Ruderman and C. Kittel, Phys. Rev. **96**, 99 (1954).

[40] T. Kasuya, Prog. Theor. Phys. **16**, 45 (1956).

[41] K. Yosida, Phys. Rev. **106**, 893 (1957).

[42] H. Hamaker, L. Woolf, H. MacKay, Z. Fisk, and M. Maple, Solid State Commun. **32**, 289 (1979).

[43] J. H. Van Vleck, *The Theory of Electric and Magnetic Susceptibilities* (Oxford University Press, London, 1932).

[44] P. Rhodes and E. P. Wohlfarth, Proc. R. Soc. A **273**, 247 (1963).

[45] M. B. Maple, Physica B (Amsterdam) **215**, 110 (1995).

[46] M. B. Maple, M. C. de Andrade, J. Herrmann, Y. Dalichaouch, D. A. Gajewski, C. L. Seaman, R. Chau, R. Movshovich, M. C. Aronson, and R. Osborn, J. Low Temp. Phys. **99**, 223 (1995).

[47] N. H. Franse, in *Crystalline Electrical Field and Structural Effects in f-Electron Systems*, edited by J. E. Crow, R. P. Guertin, and T. W. Mihalisin (Plenum, New York, 1980).

[48] N. Hessel Andersen and H. Smith, Phys. Rev. B **19**, 384 (1979).

[49] M. B. Fontes, J. C. Trochez, B. Giordanengo, S. L. Bud'ko, D. R. Sanchez, E. M. Baggio-Saitovitch, and M. A. Continentino, Phys. Rev. B **60**, 6781 (1999).

[50] M. J. Kangas, D. C. Schmitt, A. Sakai, S. Nakatsuji, and J. Y. Chan, J. Solid State Chem. **196**, 274 (2012).

[51] R. S. Fishman and S. H. Liu, Phys. Rev. B **40**, 11028 (1989).

[52] A. Mackintosh, Phys. Lett. **4**, 140 (1963).

[53] J. Van Kranendonk and J. H. Van Vleck, Rev. Mod. Phys. **30**, 1 (1958).

[54] K. R. Lea, M. J. M. Leask, and W. P. Wolf, J. Phys. Chem. Solids **23**, 1381 (1962).

[55] Y. Isikawa, T. Mizushima, S. Miyamoto, K. Kumagai, M. Nakahara, H. Okuyama, T. Tayama, T. Kuwai, and P. Lejay, J. Kor. Phys. Soc. **63**, 644 (2013).

[56] P. G. De Gennes, J. Phys. Radium **23**, 510 (1962).

[57] S. Ramakrishnan, K. Ghosh, A. D. Chinchure, V. R. Marathe, and G. Chandra, Phys. Rev. B **52**, 6784 (1995).

[58] K. Kadowaki and S. Woods, Solid State Commun. **58**, 507 (1986).

[59] N. Tsujii, H. Kontani, and K. Yoshimura, Phys. Rev. Lett. **94**, 057201 (2005).

[60] P. Gegenwart, J. Custers, Y. Tokiwa, C. Geibel, and F. Steglich, Phys. Rev. Lett. **94**, 076402 (2005).

[61] Z. Fisk, H. R. Ott, and G. Aeppli, Jpn. J. Appl. Phys. **26**, 1882 (1987).

[62] Z. Fisk, H. R. Ott, and J. L. Smith, Nature (London) **320**, 124 (1986).

[63] J.-H. Chung, M. Matsuda, S.-H. Lee, K. Kakurai, H. Ueda, T. J. Sato, H. Takagi, K.-P. Hong, and S. Park, Phys. Rev. Lett. **95**, 247204 (2005).